JOURNAL OF MATERIALS SCIENCE 25 (1990) 2447–2453

Characterization of spinel particles in zinc oxide varistors

T. ASOKAN, R. FREER
Materials Science Centre, University of Manchester/UMIST, Grosvenor Street, Manchester M1 7HS, UK

Microstructural features and elemental distribution characteristics of the spinel phase in ZnO varistors have been investigated by electron probe microanalysis and transmission electron microscopy. The distribution characteristics of minor additive elements including Co, Mn, Ni and Cr in different phases are also examined. The V–I characteristics of two types of sample, possessing identical intergranular phase, are compared and discussed in relation to the spinel characteristics.

1. Introduction

Zinc oxide varistors are sintered ceramic devices consisting mainly of ZnO with small amounts of oxide additives, such as Bi_2O_3, Sb_2O_3, CoO, MnO_2, Cr_2O_3 and NiO [1]. These varistors are known to exhibit highly non-linear voltage–current (V–I) characteristics and a high energy absorption capability, coupled with low power loss [1–3]. The combination of such properties have made ZnO varistors extremely attractive as protection devices for high power applications in recent years.

The microstructure of a ZnO varistor comprises highly conductive ZnO grains surrounded by electrically insulating grain boundary regions [4]. The presence of insulating regions, composed mainly of Bi_2O_3, is believed to be the cause of the non-linear V–I characteristics [5]. It has been established that non-Ohmic ZnO varistors contain two major accessory phases: a Bi_2O_3-rich intergranular phase and a $Zn_7Sb_2O_{12}$ spinel phase [6]. The Bi_2O_3-rich intergranular phase has been the subject of many investigations during the last decade, e.g. [7, 8], but in contrast the $Zn_7Sb_2O_{12}$ spinel phase has received comparatively little attention. As a result, there is a paucity of literature available on the chemistry and microstructure of the latter. Since more than 10% by volume of a commercial ZnO varistor is usually occupied by the spinel phase, it is desirable that we should have a better understanding of the characteristics and role of this phase.

In the present study, an attempt has been made to identify the principle microstructural features of the spinel phase. The distribution of minor elements, including Co, Mn, Cr and Ni, has been studied and the inter-relationships with ZnO grains and the Bi_2O_3-rich intergranular phase have been examined.

2. Experimental procedures

2.1. Sample preparation

Reagent grade (BDH) powders of ZnO (87.425 wt %), Bi_2O_3 (6.00%), Sb_2O_3 (3.5%), CoO (0.55%), MnO_2 (0.70%), Cr_2O_3 (0.90%), NiO (0.90%) and $Al(NO_3)_3$ (0.025%) were mixed with deionized water and milled for 5 h using agate grinding media. The charge was dried, mixed with 2% polyvinyl alcohol and formed into discs of 18 mm diameter and 3 mm thickness using a single action uniaxial press, operating at 300 kg cm^{-2}. From the single composition mixture, two types of samples, designated A and B, were obtained by varying the sintering procedure as follows:

Type A: Green compacts were sintered in air at 1250° C for 2 h and cooled with the furnace to room temperature.

Type B: Green compacts were first sintered in air at 900° C for 1 h and furnace cooled, and then sintered at 1250° C for 2 h, as in the case of Type A.

The rate of heating (3° C min^{-1}) and cooling (with the furnace), during sintering, was the same for all specimens.

2.2. Characterization

The densities of the sintered pellets were determined from mass and volume measurements, using at least 10 samples of each type. For X-ray diffraction studies, Cu$K\alpha$ radiation was used in conjunction with a Philips diffractometer (PW 1380). Before electrical characterization, the sintered samples were lapped to remove surface flaws. Ohmic contacts were applied to both surfaces by coating with colloidal (air-drying) silver paint. Standard V–I measurements were carried out using a stabilized d.c. power source in a current range upto 1 mA. The leakage current was determined at 80% $V_{1\,mA}$ level. Procedures for V–I measurements and leakage current calculation are discussed in detail elsewhere [9, 10].

2.3. Electron-probe microanalysis

The surfaces of selected sintered samples were polished down to 1 μm diamond paste and coated with carbon to a thickness of approximately 30 nm. These samples were examined in detail using an electron microprobe (Cameca-Camebax electron probe with

0022–2461/90 $03.00 + .12

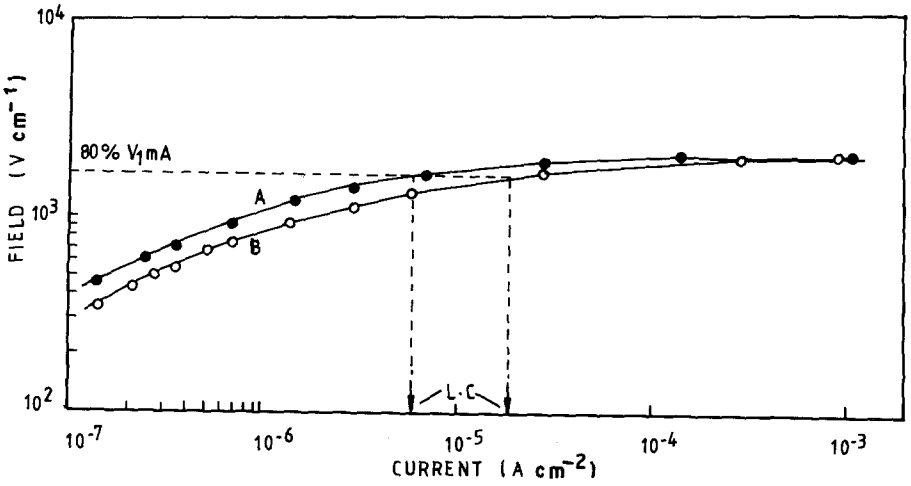

Figure 1 V–I characteristics of Type A and B samples.

Link analytical AW 10 000 EDS system), operating at 20 kV with beam current of 15 nA.

Qualitative descriptions of elemental distribution were obtained for each element of interest by repeatedly scanning selected regions. Complementary quantitative analyses were performed at 3 μm steps using energy dispersive techniques.

2.4. Transmission electron microscopy

Sintered samples were sliced and ground to a thickness of approximately 100 μm using conventional techniques. Discs of $\simeq$3 mm diameter were cut from these samples. A dimpler (Model-D500, VCR Group, Inc.) was used to reduce the thickness at the centre of the specimens to $\simeq$10 μm, and thinning completed by ion-beam milling using 3 kV Ar^+ ions). Transmission electron microscopy of representative samples was performed on a Philips EM 430 instrument with an EDAX analytical facility.

3. Results and discussion

3.1. Bulk properties

The *V–I* characteristics of Type A and B samples are shown in Fig. 1. The densities, grain size and leakage currents of the samples are summarized in Table I. It may be observed that breakdown voltages ($V_{1\,mA}$) are the same whilst the pre-breakdown behaviour differs considerably. X-ray diffraction studies did not reveal any significant differences between the samples. The phases observed were hexagonal ZnO, cubic Zn–Sb spinel and tetragonal β-Bi_2O_3.

It is interesting to note that although the density of the Type B sample is higher than that of the Type A sample, the leakage current in Type B is a factor of three higher than that in Type A. The higher leakage current in Type B samples may be related, in part, to the variation of grain size, since an increase of grain size would result in a lower total grain boundary volume. However, the net differences between the two parameters suggests that the grain size is not the only factor controlling the leakage current.

As the intergranular phase is the same in both samples, it may be inferred that this phase is not the primary cause of the variation of leakage current. The only other major phase to be considered is therefore spinel. The following sections summarize investigations of the microstructural features and elemental distributions in the spinel phase in each type of specimen.

TABLE I The density, grain size and leakage current of Type A and B samples

Type	Density ($g\,cm^{-3}$)	Grain size (μm)	Leakage current (μA)
A	4.88 ± 0.04	7.52 ± 0.03	6.0
B	5.21 ± 0.05	9.73 ± 0.04	19.0

3.2. Microanalysis of bulk specimens

Micrographs of the backscattered electron image and concentration line profiles of elements across regions of Type A and B samples are shown in Figs 2 and 3, respectively. It may be observed that antimony is distributed in the junctions of grains as well as in isolated locations within the ZnO grains (Fig. 3). The minor additive elements Mn, Cr, Ni and Co are found only in the regions where antimony is present. The antimony-rich phase in the micrograph may be identified as a spinel phase. From the X-ray diffraction and chemical analyses the spinel is anticipated to be approximately $Zn_{7/3}Sb_{2/3}O_4$.

The following conclusions may be drawn from a critical appraisal of observed phase relationships at grain junctions. In Type A samples the Bi_2O_3-rich phase is sandwiched between a spinel grain and ZnO grains, as reported earlier [11], whilst in Type B samples the Bi_2O_3-rich phase is formed only between ZnO grains. Furthermore, in Type B samples the spinel particles are dispersed in Bi_2O_3-rich phase. Typical examples of the phase distributions are shown schematically in Fig. 4, and in the SEM micrograph for Type B sample in Fig. 5. The average composition of the spinel phase in both types of sample is given in Table II.

TABLE II Typical composition (obtained by EDS analysis) of a spinel particle in a monolithic Type B sample

Oxide	Concentration (wt %)
ZnO	48.23
Sb_2O_3	31.35
Cr_2O_3	8.06
MnO_2	3.33
CoO	0.98
NiO	4.30

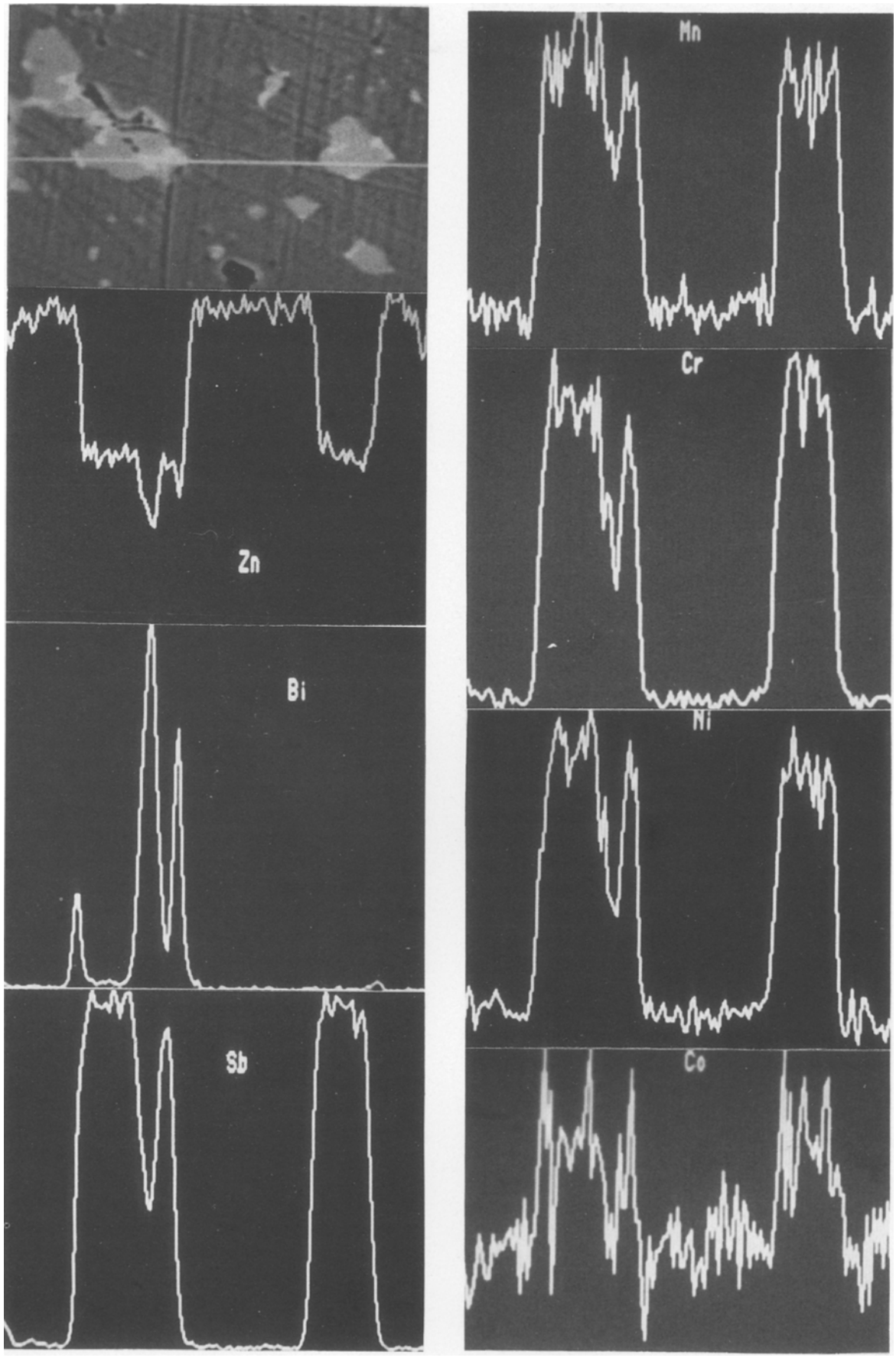

Figure 2 Backscattered electron image of a region of Type A sample and elemental concentration profiles across the line indicated on the micrograph.

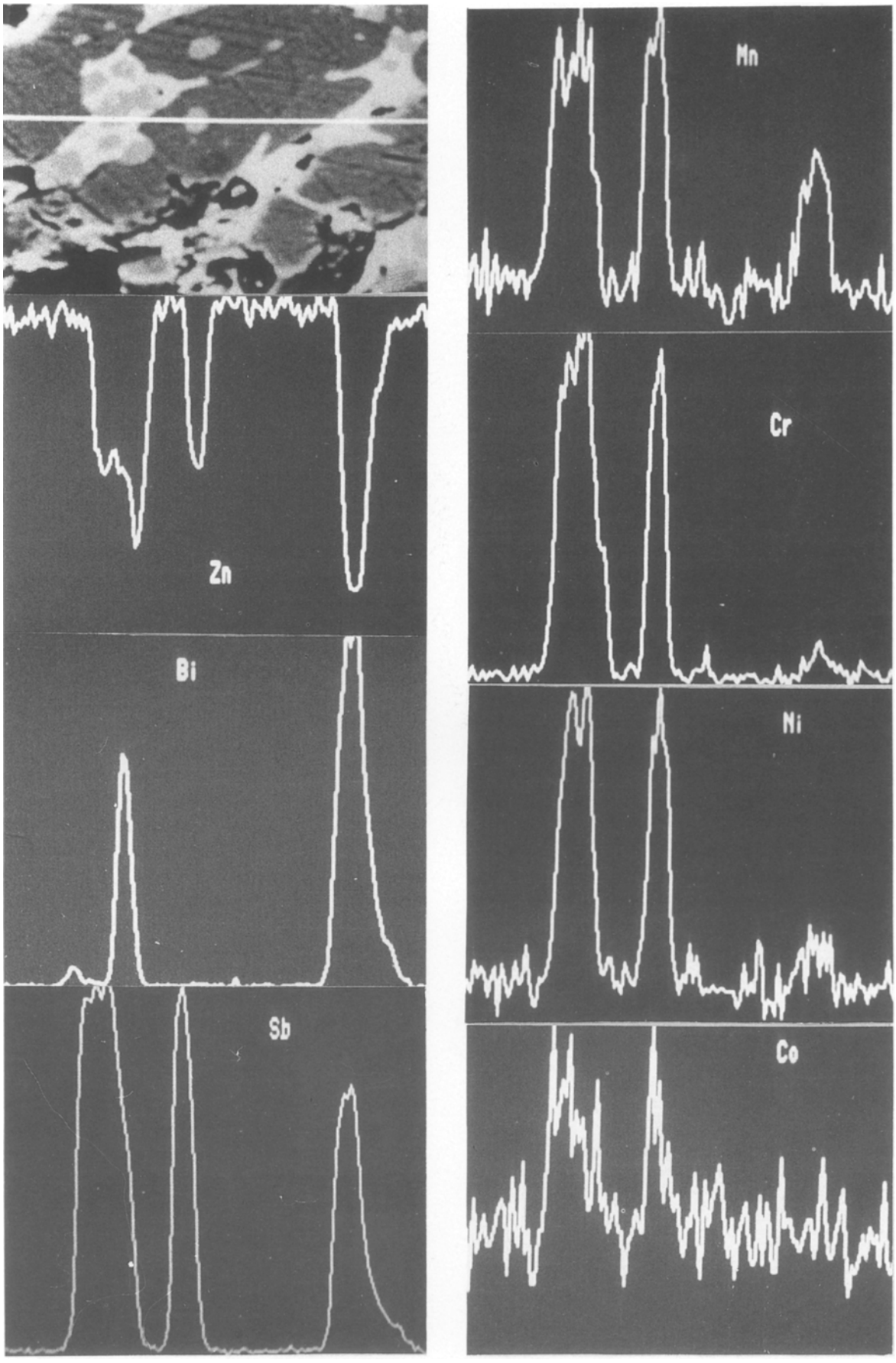

Figure 3 Backscattered electron image of a region of Type B sample and elemental concentration profiles across the line indicated on the micrograph.

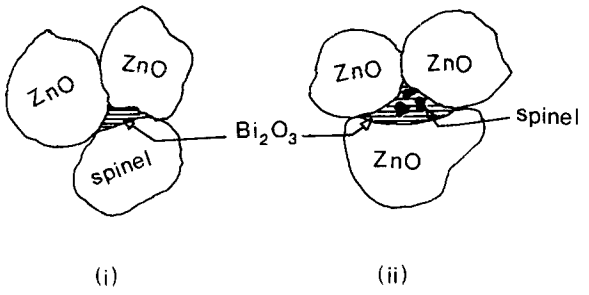

Figure 4 A schematic representation of grain junctions in (i) Type A and (ii) Type B samples.

Figs 2 and 3 show that the minor additive elements Mn, Cr, Ni and Co are concentrated in the spinel regions. Line profiles of these elements in both types of sample reveal that the Bi_2O_3-rich phase does not contain significant amounts of the minor elements. The CoO is added mainly to prevent Bi_2O_3 evaporation at higher temperatures during sintering [1]. In order to understand the dissolution of the minor elements in the major phases, the samples were analysed quantitatively.

The composition profiles for Type A sample, shown in Fig. 6, are based on electron microprobe analyses (EDS mode) using a stepping interval of 3 μm. The analyses were performed at a randomly selected, but typical grain junction. The composition profiles confirm that the minor additive elements are concentrated in the antimony-rich phase, as indicated in the qualitative line analyses. Minor element concentrations in the Bi_2O_3-rich phase appear to be 0.3–0.5 wt %. These levels may be an artefact of the analysis and enhanced by fluorescence effects from neighbouring ZnO or spinel grains, or indeed regions below the thin Bi_2O_3 phase. It is therefore expected that the true concentration of minor elements in the Bi_2O_3 may be less than 0.3 wt %. In order to confirm the minor element concentrations, complementary studies of thin specimens were performed.

3.3. Microanalysis of thin specimens

Transmission electron micrographs from Type A and B samples are shown in Figs 7 and 8. Energy dispersive compositional analyses were performed at

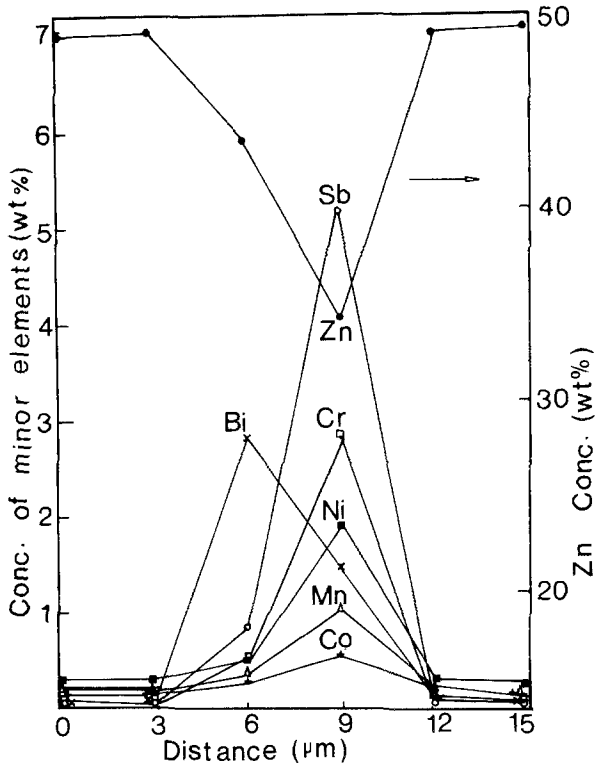

Figure 6 Quantitative concentration profile of elements at the junction of grains in Type A samples.

selected locations. The principle phases are indicated in the micrographs. It is interesting to note in Type A samples that triple points (Bi_2O_3-rich phase) exist between two ZnO grains and a spinel grain. In contrast, in the type B sample (Fig. 8) the triple point (Bi_2O_3-rich phase) is formed only between ZnO grains. These results support the qualitative data obtained with bulk specimens (see section 3.2). In addition, in both Type A and B samples, isolated spinel grains are also found within ZnO grains (Fig. 7).

Fig. 9 shows the microstructure of a spinel grain adjacent to a triple point, in Type A sample. The spinel grain is associated with a number of line defects (dislocations). These defects were not found in the Type B samples. Instead, an additional minor phase was observed (Fig. 10). This was not detected by X-ray diffraction analysis because of the small total

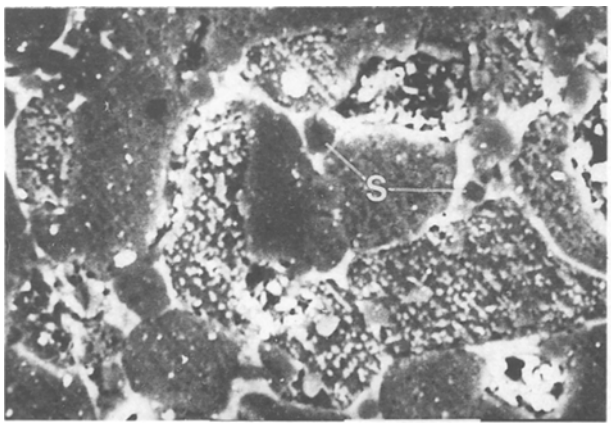

Figure 5 Scanning electron micrograph of Type B sample (bar = 10 μm, S ≈ spinel).

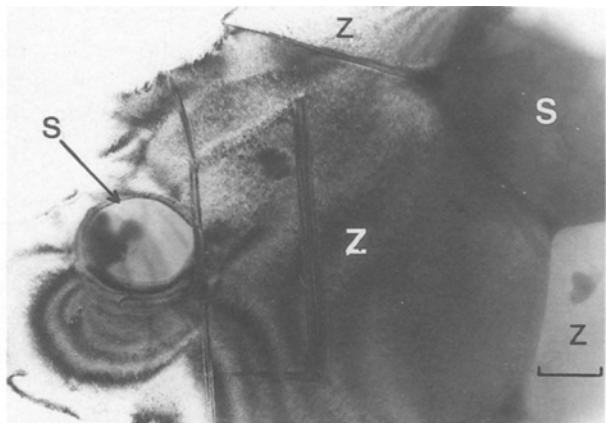

Figure 7 Transmission electron micrograph of Type A sample (bar = 0.5 μm, Z = ZnO, S = spinel, B = Bi_2O_3).

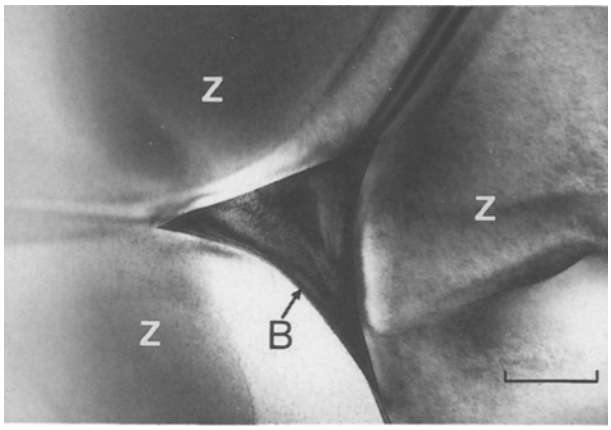

Figure 8 Transmission electron micrograph of Type B sample (bar = 0.5 μm, Z = ZnO, B = Bi_2O_3).

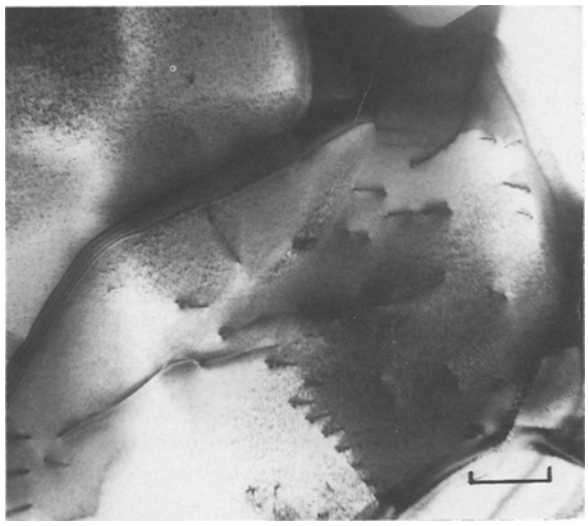

Figure 9 Transmission electron micrograph of Type A sample showing dislocations in spinel grain (bar = 0.5 μm).

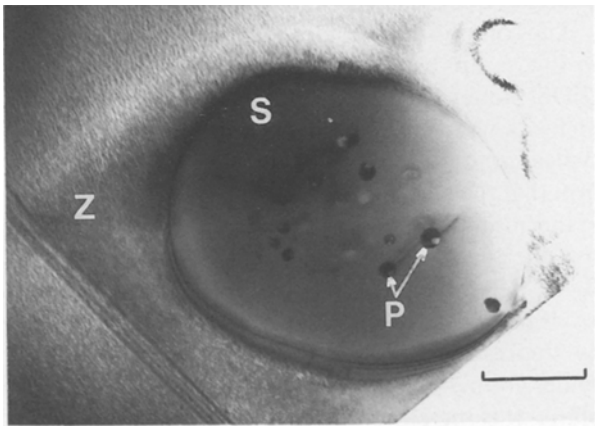

Figure 10 Transmission electron micrograph of spinel particle containing Zn–Bi–Sb pyrochlore phase in Type B sample (bar = 0.5 μm, Z = ZnO, S = spinel, P = pyrochlore).

volume of the phase. The composition, determined by EDAX, is: Bi_2O_3 (47.13 wt %), ZnO (28.79%), Sb_2O_3 (17.00%), Cr_2O_3 (2.76%), NiO (2.11%), CoO (0.67%) and MnO_2 (1.52%). This may be identified as a Zn–Bi–Sb pyrochlore phase, of approximate formula $Zn_2Bi_3Sb_3O_{14}$. A phase of this kind was not observed in Type A samples. It is of interest to note that the ZnO regions near the spinel particles in both types of sample frequently contain planar defects (Figs 7 and 10). Rapid shrinkage of the spinel phase during sintering, accompanied by the dissolution of the minor additives may be the cause of planar defect formation in the ZnO region.

Analyses of the various phases are summarized in Table III. Results for Type A and B samples are not significantly different. The following trends may be identified:

(a) Minor additive elements such as Co, Ni and Mn dissolve in ZnO grains. The concentration of Co is significantly higher than that of the other two elements.

(b) The spinel phase contains all the minor additive elements. Dissolved Cr is only found in the spinel phase.

(c) The Bi_2O_3 phase (triple point region) does not contain measurable quantities of many minor additive elements.

Since Co was not detected in the Bi_2O_3 phase, it would appear that Bi_2O_3 evaporation at higher temperature, is controlled by factors other than solid solution formation with cobalt.

These investigations therefore show that the elemental distribution characteristics of the spinel phase can be modified considerably by varying the sintering procedures. It is believed that the microstructural characteristics of the spinel, the formation of line defects and the Bi–Zn–Sb pyrochlore phase in spinel can influence the electrical properties of the material as demonstrated in Type A and B samples.

4. Conclusions

(a) The *V–I* characteristics of a ZnO varistor are influenced not only by the Bi_2O_3 intergranular phase but also by the characteristics of the spinel phase.

TABLE III Typical compositions (obtained by EDS analysis) of phases in Type A and B samples

Oxide	ZnO grain		Spinel		Triple point	
	A	B	A	B	A	B
ZnO	99.09	98.7	54.51	52.72	–	–
Bi_2O_3	–	–	–	–	99.43	98.93
Sb_2O_3	–	–	29.79	31.81	–	–
Cr_2O_3	–	–	6.19	7.01	–	–
CoO	0.57	0.62	1.44	1.15	–	–
MnO_2	0.16	0.35	2.74	2.43	–	–
NiO	0.18	0.37	5.31	4.86	–	–

(b) The spinel phase is formed both in the junctions of the grains and also within ZnO grain. The relationships of spinel–ZnO–Bi_2O_3 phases in the junctions can be modified considerably by the sintering procedure.

(c) The minor additive elements dissolve in the spinel phase as well as in ZnO. The intergranular phase (Bi_2O_3) does not contain significant levels of additive elements.

(d) The Zn–Bi–Sb pyrochlore phase is distributed within the spinel regions.

Acknowledgement

Support for this work by the Science and Engineering Research Council is gratefully acknowledged. The authors wish to thank Mr D. A. Plant, Mr G. Cliff and Mr I. Brough for their assistance with specimen analysis and Mr I. Owate for help with the preparation of the manuscript.

References

1. M. MATSUOKA, *Jpn J. Appl. Phys.* **10** (1971) 736.
2. E. C. SAKSHAUG, J. S. KRESGE and S. A. MISKE JR, *IEEE Trans. Power Appar. Syst.* **PAS-96** (1977) 647.
3. S. TOMINAGA, Y. SHIBUYA, Y. FUJIWARA and T. NITTA, *IEEE PES Summer Meeting* **A78** (1978) 595.
4. L. M. LEVINSON and H. R. PHILIPP, *J. Appl. Phys.* **46** (1975) 1332.
5. K. EDA, *J. Appl. Phys.* **49** (1978) 2964.
6. R. EINZINGER, *Ann. Rev. Mater. Sci.* **17** (1987) 299.
7. J. WONG, *J. Appl. Phys.* **51** (1980) 4453.
8. R. EINZINGER, "Grain boundary phenomena in Electronic Ceramics, Advances in Ceramics", Vol. 1, edited by L. M. Levinson (1981) p. 359.
9. T. ASOKAN, G. R. NAGABHUSHANA and G. N. K. IYENGAR, *IEEE Trans. Elec. Insulation* **23** (1988) 279.
10. T. ASOKAN, G. N. K. IYENGAR and G. R. NAGABHUSHANA, *J. Amer. Ceram. Soc.* **70** (1987) 643.
11. H. CERVA and W. RUSSWURM, *J. Amer. Ceram. Soc.* **71** (1988) 522.

Received 19 January
and accepted 31 May 1989